

Aircraft Engine Technology - Report III
Transatlantic Ground Effect Vehicle

Department of Mechanical Engineering
Imperial College London

Monday 9th March 2020

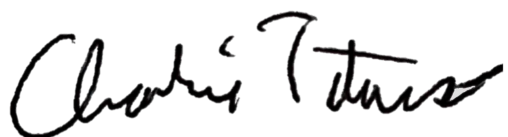
We declare that an equal contribution to this report has been made by all group members and we agree to an equal distribution of marks.



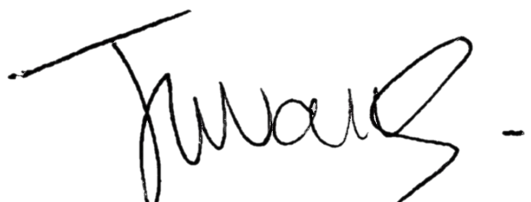
Thomas John Fisher
01067451



Henry Hart
01190775



Charles Titmuss
01213323



Joseff Williams
0106765

Abstract

As the world economy increasingly makes moves towards the decarbonisation of transport, a more efficient, fast form of transatlantic transport is required. One possible solution could be a vehicle which uses the ground effect to fly with a higher L/D ratio than a typical airliner, and as a result consumes less fuel over the course of a transatlantic journey.

This report details the design process undertaken and the results obtained for the design of the main engines for a ground effect vehicle based loosely on the soviet era Lun Class Ekranoplan airframe. The L/D ratio for the vehicle was calculated for an appropriate flight height and this was then used to specify the optimal flight speed. This then allowed a thermodynamic jet engine cycle to be designed using the Gasturb software suite.

This cycle was then used to design the number of stages and geometry of the turbomachinery for the engine. The proposed design is a twin shaft turbofan engine with a bypass ratio of 13. The core consists of a single stage booster, an 11 stage high pressure compressor, a 2 stage high pressure turbine, and a 5 stage low pressure turbine. In general, the geometry of the design was chosen so as to be in keeping with industry accepted best practice and to keep aerodynamic losses to a minimum.

A full engine schematic is presented along with the blade flow angles for the final stages of the high pressure compressor and turbine. This disk stresses where also computed for the high pressure turbine stages.

It was found that by using the 1970s air-frame of the Ekranoplan it was not possible to achieve L/D ratios significantly higher than a modern airliner. As a result, despite a low specific fuel consumption for the engine the resulting aircraft was not capable of flying a comparable journey with less fuel than a modern airliner. Modern airliners have significantly higher L/D ratios than their 1970s equivalents and it is suggested that a more modern ground effect capable airframe may allow similar ground effect benefits to be achieved but with higher L/D ratios than the Ekranoplan airframe would allow.

Contents

1	Introduction	1
1.1	Motivations	1
1.2	Design aims	1
1.3	The Ekranoplan Project	1
2	Design Condition	2
2.1	Airframe Parameters	2
2.2	Selection of Cruise Height	2
2.3	Cruise Velocity	3
2.4	Thrust and Mass Flow	5
2.5	Cooling Air	6
3	Off-design	7
3.1	Out of Ground Effect	7
3.2	Five-Engine Out of Ground Effect Flight	7
4	Engine Cycle Design	8
4.1	Optimisation process	8
4.2	Results and Proposed Specification	9
5	Turbomachinery Design	11
5.1	Fan	11
5.2	Booster Stage	12
5.3	High Pressure Compressor	13
5.4	Turbines	13
5.5	Nozzle outlets	14
6	Blade Geometry	16
7	HPT Disc Stresses	19
8	Conclusions & Further Work	23
9	References	24
A	Gasturb Outputs	A-1
A.1	On-Design Cruise Condition	A-1
A.2	Cruise Condition, Five Engines	A-2
A.3	Out of Ground Effect, Minimum Thrust, Six Engines	A-3
A.4	Out of Ground Effect, Minimum Thrust, Five Engines	A-4
B	Engine Schematic	B-1

Nomenclature

$(1 - \sigma)$	Induced drag factor;	F_{sp}	Specific thrust;
α	Absolute flow angle;	h	Cruise height;
\bar{m}	Non-dimensional mass flow rate;	h_s	Significant wave height;
β	Flow angle relative to blade;	h_{max}	Maximum wave height;
\dot{m}	Mass flow rate;	K	Constant for lift-drag polar;
η_{mech}	Mechanical efficiency;	k	Constant for nacelle friction;
η_p	Polytropic efficiency;	L	Lift;
η_s	Isentropic efficiency;	l	End plate depth;
γ	Ratio of specific heats;	m_b	Blade mass;
ν	Poisson's ratio;	Ma	Mach number;
ω	Shaft angular velocity;	n	Number of blades;
ϕ	Flow coefficient;	P_o	Stagnation pressure;
ψ	Work coefficient;	R	Hub radius;
ρ	Air density;	R	Universal gas constant;
σ_r	Radial stress;	r_A	Aspect ratio;
σ_θ	Hoop stress;	R_i	Inner radius of the disk;
$\tilde{\sigma}$	Tresca stress;	R_m	Blade mean radius;
A	Annulus area;	R_o	Outer radius of the disk;
a	Speed of sound;	r_p	Pressure ratio;
A_{fan}	Fan area;	R_r	Blade root radius;
b	Wingspan;	R_t	Blade tip radius;
c	Blade chord length;	S	Wing area;
C_D	Coefficient of drag;	s	Blade pitch;
C_L	Coefficient of lift;	T	Temperature;
c_p	Specific heat at constant pressure;	t	Blade thickness;
c_θ	Tangential axial velocity;	t_d	Disk thickness;
C_{D0}	Zero lift drag;	T_o	Stagnation temperature;
D	Drag;	T_R	Required thrust;
D_{tip}	Fan diameter;	TET	Turbine entry temperature;
DF	Lieblien diffusion factor;	U_m	Mean radius blade velocity;
E	Elastic modulus;	V_∞	Flight velocity;
F_N	Net thrust;	V_x	Axial velocity;
F_{rim}	net force on the rim;	W	Weight;
$F_{sp,eff}$	Effective specific thrust;	z_w	Zweifel coefficient;
			MTOW Maximum take-off Weight;

1 Introduction

This project has considered the outline design for the main engines of a new type of long haul aircraft. The aircraft is loosely based on an Ekranoplan Lun Class and is intended as an efficient alternative to long haul transatlantic aircraft, providing high efficiency for a large payload mass. The focus of this report is on the design and specification of the main engines for the Lun Class rather than the booster engines that are required in order to get the craft airborne. This report sets out the design condition and off-design requirements for this engine; specifies its thermodynamic cycle; and outlines the design of the turbomachinery, including the number of stages required, the blade geometry and the stress analysis of the high pressure turbine disc. Finally, an outline schematic of the engine is presented.

1.1 Motivations

Currently, around 50 million transatlantic journeys are offered by airlines each year. Whilst ideally, all fossil fuelled transport between Europe and the Americas would be phased out over the medium term, there will always be a demand for transatlantic journeys at speeds greater than that of a ship. Currently the options are limited. Conventional long haul flight is the most common current solution. It is fast, with a London to New-York journey taking just 8 hours, but this is one of the most carbon intensive means of transport [EEA, 2014]. Alternately, marine transport offers a much longer journey time (days or weeks) but a far lower CO₂ contribution [EEA, 2014]. Efforts to reduce this journey time in ships have met considerable technical barriers, such as cavitation of flow about hydrofoils.

For most customers, travelling for either business or leisure, a transatlantic journey time greater than one day is likely to be highly prohibitive. This motivates the investigation into a more efficient form of ‘flight’ using a Ground Effect Vehicle (GEV) which has the potential to leverage a higher lift to drag ratio than a conventional airliner due to the aerodynamic ground effect. This proposed vehicle would constitute a compromise between speed and efficiency.

1.2 Design aims

It is envisaged that the proposed aircraft will be capable of making the 5,600 km journey from London to New-York in less than 24 hours, and have a lower total fuel consumption per passenger over the journey than a typical airliner.

1.3 The Ekranoplan Project

There have been a number of previous attempts at designing GEVs of this scale, the most notable of which undertaken by the Soviet and Russian navies in the 1970s, 80s and 90s. The Lun Class Ekranoplan was designed and built to travel across the Caspian sea at a far higher speed than a conventional floating vessel, but with a higher payload capacity than a conventional aircraft [Yun et al., 2010]. One Lun class craft was built in 1987 and operated into the 1990s. A second was commissioned to act as a mobile hospital, but was never finished.

2 Design Condition

2.1 Airframe Parameters

The airframe considered herein is loosely based on the Lun Class Ekranoplan, as designed by the Soviet Navy in 1975. The key physical specifications of the proposed air frame are given in table 1.

Table 1: Key specifications of the proposed air frame

Particular	Value
Max take-off Weight (MTOW) [t]	380
Wingspan (b) [m]	80
Wing-area [m^2]	1800

The proposed air-frame has a significantly larger wing-span to the original Lun Class, of 80 m compared to 60 m respectively. This is in order to allow it to fly in the ground effect at greater altitude than than the Lun Class, enabling it to clear the larger waves expected in the Atlantic ocean compared to the Caspian sea (for which the Lun Class was designed).

The max take off weight was selected as that of the Lun Class. Whilst the modified craft does have a larger wingspan than the original craft, this is justifiable within the same total weight as mechanical design has improved significantly since the 1970s with new engineering alloys and more sophisticated analysis methods producing lighter airframes.

The proposed GEV will be powered by six two-spool, high-bypass turbofan engines, at the cruise condition. The take off condition for a GEV is considerably more onerous relative to the cruise condition when compared to a traditional airliner. Additional drag due to hydrodynamic forces is large compared to the aerodynamic forces experienced when in flight and so it is typical for additional "booster" engines to be used during the take off condition. This allows the main engines to be better optimised at the cruise condition thus increases the range and efficiency of the craft. This was the approach favoured in the design of the original Ekranoplans by the Soviet Navy, such as the A-90 Orlyonok, Lun Class and Caspian Sea Monster. The precise specification of these booster engines and the calculation of the required take-off thrust is a highly complex problem, and outside of the scope of this project.

2.2 Selection of Cruise Height

The ground effect is a phenomenon whereby the lift created by an aerofoil increases when it is in close proximity to the ground. This is driven by two factors. Firstly, the ground interrupting the formation of wing tip vortices. This reduces the drag due to the aerofoil. Additionally, the close proximity of the ground increases the pressure on the lower face of the wing increasing the resulting lift. The combination of these two factors causes the lift to drag ratio to increase. With the ground closer to the wing both of these factors are increased resulting in a higher L/D ratio at lower cruise heights.

This means that the selection of cruise height is critical in the design of a GEV. Higher flight results in a less favourable lift to drag ratio, yet the cruise height must still be sufficient for the GEV to clear most waves on the ocean. Therefore, in order to maximise efficiency, cruise height must be set to the lowest safe value.

This criteria was set as a cruise height that would be safe to fly at for 80% of the time over the North Atlantic Ocean in winter, which implies a cruise height of 13.45 m. This value was calculated from the data collected at a meteorological station in the North Atlantic over a 5 year continuous period and given in Lin and Dong [2019]. A 1.5 m airgap was included over h_{max} as is typical in the design of offshore platforms [SNAME, 2008]. This should ensure that the aircraft can expect to operate at its design point (cruise) for at least 80% of the flight. Should large waves be forecast, the aircraft can climb

away from danger, flying at a greater altitude but incur a penalty in specific fuel consumption, due to a reduced L/D .

Data given in Lin and Dong [2019] describes the probability density function (PDF) of the significant wave height as measured the the North Atlantic. The distribution was modelled as a modified maximum entropy distribution as formulated in Zhang and Xu [2005], with a PDF as given in equation 1. Γ^{-1} is the inverse gamma distribution, evaluated as 2.716×10^{-14} in this case.

$$f_X(h_s) = \xi \beta^{\frac{\gamma+1}{\xi}} \Gamma^{-1} \left(\frac{\gamma+1}{\xi} \right) (h_s - a_o)^\gamma e^{-\beta(h_s - a_o)^\xi} \quad (1)$$

For the most onerous winter months,

$$\beta = 9.8511, \quad \gamma = 6.0096, \quad \xi = 0.4075, \quad a_o = 0.7531$$

These values were calculated using a minimum likelihood estimation optimisation method for the empirical data gathered. This distribution was then used to calculate the cumulative probability and is plotted in figure 1. This indicates a 80th percentile winter significant wave height of 6.82 m.

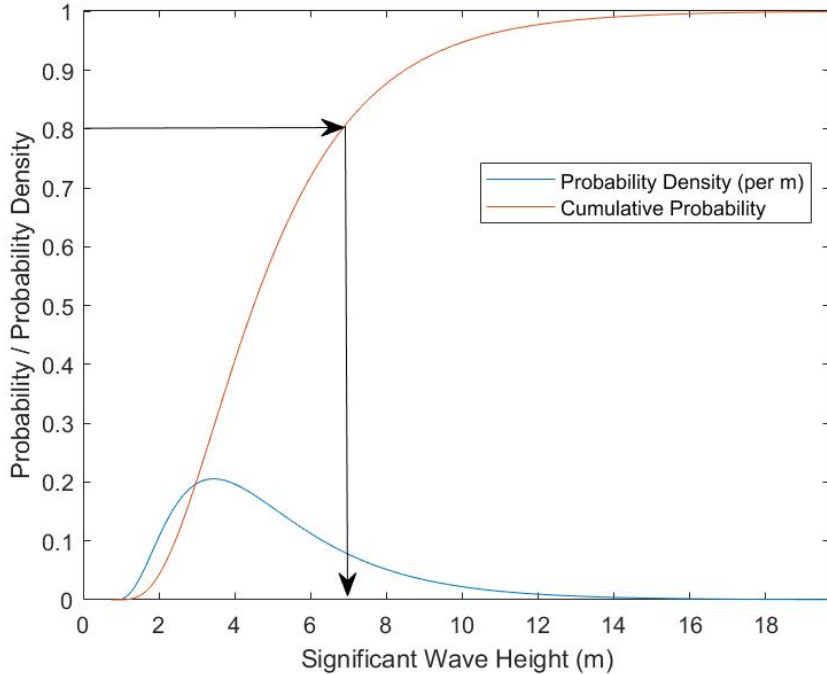


Figure 1: PDF and CDF of wave heights for North Atlantic in Winter

The maximum wave height can then be calculated using the ratio h_{max}/h_s suggested by SNAME, 2008 of 1.75 for cyclonic areas. This gives a cruise flight height of 13.45 m, as shown below.

$$h = 1.75h_s + \text{airgap} = 1.75 \times 6.82 + 1.5 = 13.45 \text{ m} \quad (2)$$

2.3 Cruise Velocity

The purpose of the ground effect vehicle is to reduce the environmental impact of long haul transatlantic travel, thus the fuel consumption must be minimised per unit distance travelled. The fuel consumed per unit distance travelled is minimised when the following function is maximised [Martinez-Botas and Davies, 2019b]:

$$\frac{T_R}{V_\infty} = \frac{D}{V_\infty} = \frac{1}{2} \rho V_\infty S C_D = \left(\frac{\rho W}{2S} \right)^{1/2} S \frac{C_D}{C_L^{1/2}} \quad (3)$$

In order to maximise this function we must choose a cruise velocity which maximises $C_D/C_L^{1/2}$ as all of the other parameters are fixed for a given airframe. The drag coefficient of the aircraft can be calculated as the sum of the induced drag and the zero lift drag by equation 4.

$$C_D = C_{D,0} + K C_L^2 \quad (4)$$

Combining this with the definitions of the lift and drag coefficients, equations 5 and 6, the optimal flight velocity in order to achieve maximum $C_D/C_L^{1/2}$ can be expressed as equation 7.

$$C_L = \frac{L}{\frac{1}{2} \rho v^2 S} \quad (5)$$

$$C_D = \frac{D}{\frac{1}{2} \rho v^2 S} \quad (6)$$

$$V_{max} L^{1/2}/D = \left(\frac{2}{\rho} \sqrt{\frac{3K}{C_{D,0}}} \frac{W}{S} \right)^{1/2} \quad (7)$$

For a wing in ground effect, Mantle [2016] tells us that,

$$K = \frac{(1 - \sigma)}{\pi r_A} \quad (8)$$

Where $(1 - \sigma)$ is the induced drag factor. Mantle [2016] showed that this is a function of the flight height normalised by the wingspan and the geometry of the vehicle. This plotted for a range of geometries in figure 2.

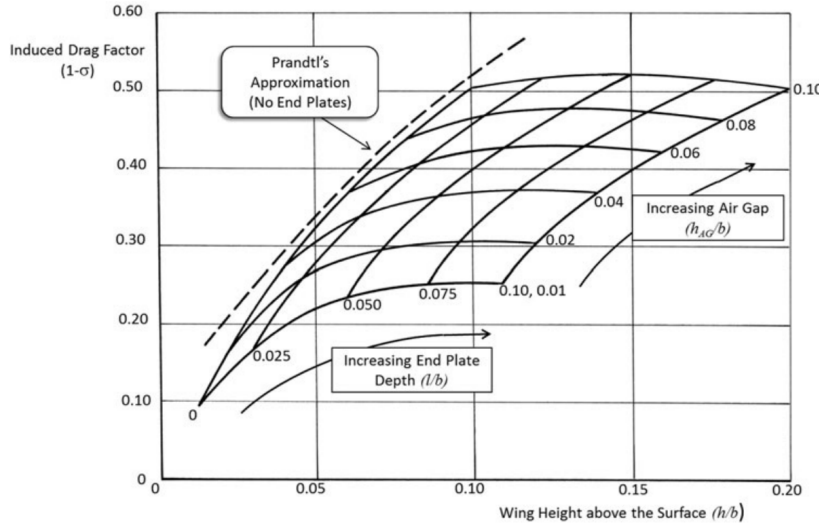


Figure 2: Induced drag factor against normalised flight height Mantle [2016]

From figure 2 $(1 - \sigma)$, was taken to be 0.49. This was based on h/b of 0.16 and end plate depths, l/b , of 0.075. With a flight height of 13.45 m, wingspan of 80 m and a wing aspect ratio, r_A of 3.53 (as per the Lun craft [Mantle, 2016]), this gives,

$$K_{GE} = 0.044$$

for the cruise case when the vehicle is flying in ground effect.

$C_{D,0}$ was taken as 0.022 as per Mantle [2016]. This gives rise to an optimal cruise velocity of,

$$V_{max \ L^{1/2}/D} = 1.316 \left(\frac{2}{1.225} \sqrt{\frac{3 \times 0.070}{0.022}} \frac{380 \times 10^3 \times 9.81}{1800} \right)^{1/2} \text{ m s}^{-1} = 90.8 \text{ m s}^{-1}$$

This is equivalent to a Mach number of 0.267. As fuel is burned over the course of a flight, the weight of the craft decreases. This is accounted for in a typical airliner by increasing the cruise altitude in order to maintain optimal L/D. For the GEV considered herein, this is not practical as it will cause the craft to fly too high to benefit from the ground effect. Instead it is proposed that the flight velocity is reduced over the course of the flight. This is considered to be acceptable as a longer flight-time compared to a commercial airliner is to be expected for the GEV.

2.4 Thrust and Mass Flow

For a 6 engine craft, the thrust required at cruise per engine was calculated from the MTOW and the L/D ratio as per equation 9.

$$F_N = \frac{MTOW}{6} \frac{1}{L/D} \quad (9)$$

The L/D ratio for the air-frame is equivalent to C_L/C_D which was calculated from equations 4 and 5. For the GEV travelling at a constant velocity, the thrust and the drag must be equal, and the lift must be equal to the total weight. The most conservative case here is when the weight is equal to the MTOW (i.e. no fuel has been burned and the payload is at its maximum). The specific thrust is then calculated from the net thrust by dividing through by the mass flow of air such that,

$$F_{sp} = \frac{F_N}{\dot{m}_{air}} \quad (10)$$

For the mach number calculated in section 2.3 the non-dimensional mass flow rate of air into the engine is given by equation 11. γ was taken as 1.4 throughout.

$$\bar{m} = \frac{\dot{m}_{air} \sqrt{c_p T_o}}{AP_o} = Ma \frac{\gamma}{\sqrt{\gamma - 1}} \left(1 + \frac{\gamma - 1}{2} M^2 \right)^{-\frac{\gamma + 1}{2(\gamma - 1)}} \quad (11)$$

The effective specific thrust is the required thrust needed to overcome the nacelle drag and losses from the inlet and outlet ducts. This was calculated in accordance to the approach detailed in Cumpsty and Heyes [2015], using equations 12 and 13. k , an empirical constant defined by the nacelle geometry was taken as 0.04.

$$F_{sp,eff} = F_{sp} \left(1 - \frac{kV}{F_{sp}} \right) \quad (12)$$

$$\dot{m}_{eff} = \frac{F_N}{F_{sp,eff}} \quad (13)$$

This was then used to compute the required fan area of each engine as per equation 14.

$$A = \frac{\dot{m}_{eff} \sqrt{C_p T_{02}}}{\bar{m} P_{02}} \quad (14)$$

Where T_{02} is given as per figure 6. The fan diameter is then a function of the fan area and blade radius, as given in equation 15.

$$D_{tip} = \frac{\sqrt{4A_{fan}}}{\pi(1 - R^2)} \quad (15)$$

The nature of the vehicle's close proximity with the sea when flying means that the engine must be installed above the wing to limit salt water spray ingress into the fan. This means that there are no ground clearance limits in fan diameter for the GEV. However, in order to limit weight and prevent excessive fan tip speeds the fan diameter will be limited to 2.5 m.

2.5 Cooling Air

Cooling air management in the engine is shown in figure 3. In order to ensure that blade temperatures remain within acceptable limits, 5% of the airflow from the core is taken out immediately before the combustor and used to cool the nozzle guide vane (which are the blades that guide the flow immediately before the high pressure turbine). A further 6% of the flow before the combustor is used to cool the high pressure turbine. The air pressure of the air cooling the HPT will therefore be higher than the rest of the flow around it. However, as it makes up only a small proportion of the overall airflow and therefore effects are negligible.

2% of the high pressure turbine airflow is used to cool the LPT in order to keep the temperatures in the blade to a reasonable level. Again, the pressure of the cooling air will be higher than that of the flow at the point of injection, but the proportion of higher pressure air is negligible.

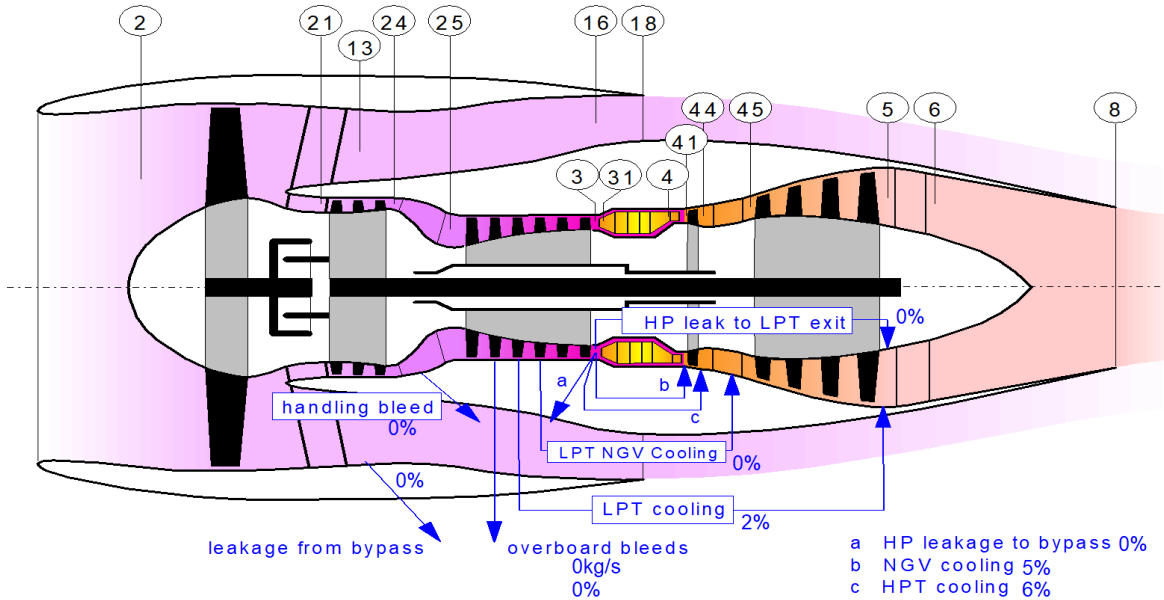


Figure 3: Schematic of the engine with cycle points labeled;

3 Off-design

In addition to ensuring that the engine is performing optimally at the design condition, several off design conditions must be considered to ensure that the aircraft can maintain flight should one engine fail, or if it is necessary to increase altitude. The most challenging of these conditions is flying out of the ground effect with a single engine malfunction. Additional conditions that will be considered will be flying out of the ground effect with all engines and flying at cruise with a reduced number of engines.

3.1 Out of Ground Effect

In order to avoid obstacles such as ships as well as escaping rough sea conditions the Ekranoplan must be capable of flight outside of the ground effect. In order to determine the change in the lift-drag characteristic associated with climbing out of ground effect, the limit of Prantl's approximation, as shown in figure 2, has been taken for large (infinite) height. Prantl's approximation is given by the following equation [Mantle, 2016]:

$$\sigma = \frac{1 - 1.32 \frac{h}{b}}{1.05 + 7.4 \frac{h}{b}} \quad (16)$$

Out of ground effect, $h \gg b$, thus at the limit of equation 16, $\sigma = -0.177$. Using equation 8, this gives rise to a K out of ground effect of,

$$K_{OOGE} = 0.1057$$

Using an equivalent method as used in equation 2.3, the cruise velocity outside of ground effect for optimal fuel consumption is given as,

$$V_{max \ L^{1/2}/D} = 114 \text{ ms}^{-1} \quad (17)$$

3.2 Five-Engine Out of Ground Effect Flight

Should one engine malfunction at any point during the flight the vehicle must still be capable of flying the aircraft outside of the ground effect. This off-design condition will be the point against which the engine is assessed in order to ensure that it is capable of holding the aircraft at this safe altitude.

When one of the engines is down and weather forces the GEV to fly out of ground effect conditions, the flight velocity for minimum thrust can be found by maximising L/D and is given by equation 18 [Cumpsty and Heyes, 2015],

$$V_{max \ L/D} = \left(\frac{2}{\rho} \sqrt{\frac{K}{C_{D,0}}} \frac{W}{S} \right)^{1/2} \quad (18)$$

This gives rise to a flight speed of,

$$V_{max \ L/D} = 86.9 \text{ ms}^{-1}$$

4 Engine Cycle Design

4.1 Optimisation process

Once the required operating conditions have been defined for the cruise condition, the specifics of the engine were calculated through an iterative procedure as shown by Figure 4. All engine optimisations and calculations were performed using the Gaturb 10 software package.

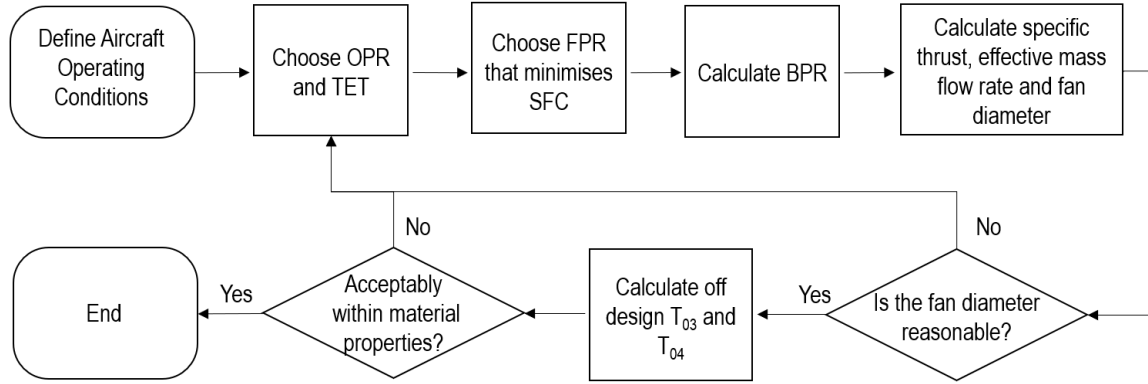


Figure 4: Flowchart detailing the optimisation process undertaken herein;

Initially, the compressor pressure ratios and turbine entry temperature (TET) were proposed. Following this, a parametric study was performed, with fan pressure ratio (FPR) as the free variable, in order to calculate optimal specific fuel consumption (SFC) and corresponding bypass ratio. A schematic plot of this optimisation can be seen in Figure 5.

With above parameters set, a single cycle study was run in order to check that the ratio of core and bypass jet velocities, V_{18}/V_8 were acceptable. If they were acceptable as denoted by Gasturb, the mass flow rate into the engine was scaled appropriately until the engine generated sufficient thrust to satisfy the conditions at cruise. If not, the TET and HPR were adjusted until the velocity ratio was acceptable. Following this, the mass flow rate was used to size the fan, and check it was within acceptable limits.

For the desired cruise net thrust of 45 kN, minimum SFC occurs at a corresponding FPR and BPR of 1.16 and 13 respectively.

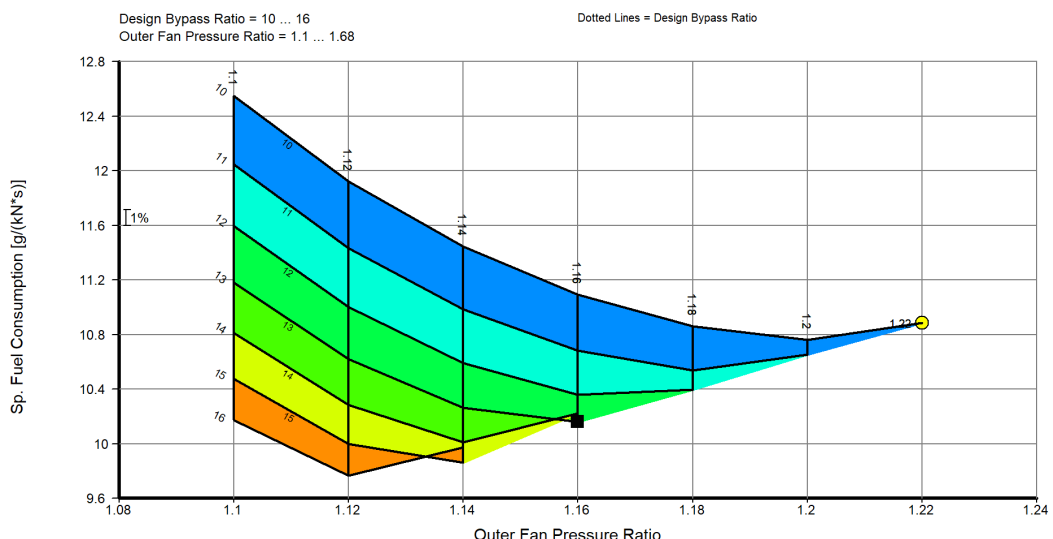


Figure 5: Specific fuel consumption for a range of bypass and fan pressure ratios;

Following this, the off-design conditions were considered. The only way for an engine to increase its thrust is to increase the TET, by burning more fuel, meaning that the maximum engine thrust is limited by the maximum TET that the engine can withstand. The most rigorous case was that of flight out of ground effect with only five engines. An optimisation study was used, with the TET limited to the maximum of 1850K and the engine parameters kept constant with an adjusted altitude and flight speed. If the thrust from the engine was insufficient, or the compressor exit temperature (CET) exceeded 950K then it was necessary to start the process again, by adjusting the OPR and TET. This in turn limited the BPR, as in order to have a large variation in thrust it is necessary to rely on flow acceleration through the core. A lower BPR allowed a larger variation in thrust, but also increased the SFC, which was undesirable. Therefore, the resulting parameters chosen minimised the SFC, while also ensuring that sufficient thrust could be generated by the engine.

The final engine design operates at a cruise SFC of $10.2 \text{gs}^{-1} \text{kN}^{-1}$, with a TET of 1271K and an OPR of 18.1. The TET was set at this relatively low value due to the need to dramatically increase thrust when operating out of ground effect. The difference in thrusts between altitudes meant that there needed to be a large increase in burner temperature between on and off design-points. This meant that in order to not exceed 1850K at the turbine while at high altitudes, cruise TET must be set at a low value. The OPR was largely constrained by engine diameter and compressor blade size. Due to the high air density at cruise, the engine is naturally smaller for a given air mass flow rate. This means that in order to keep the compressor blades at a reasonable size, the OPR must be limited. The SFC is low by similarly-purposed modern aircraft standards. However it is worth noting that the design uses 6 engines, therefore, the efficiency may in-fact be comparable to conventional craft. The T-S diagram is given in Figure 6.

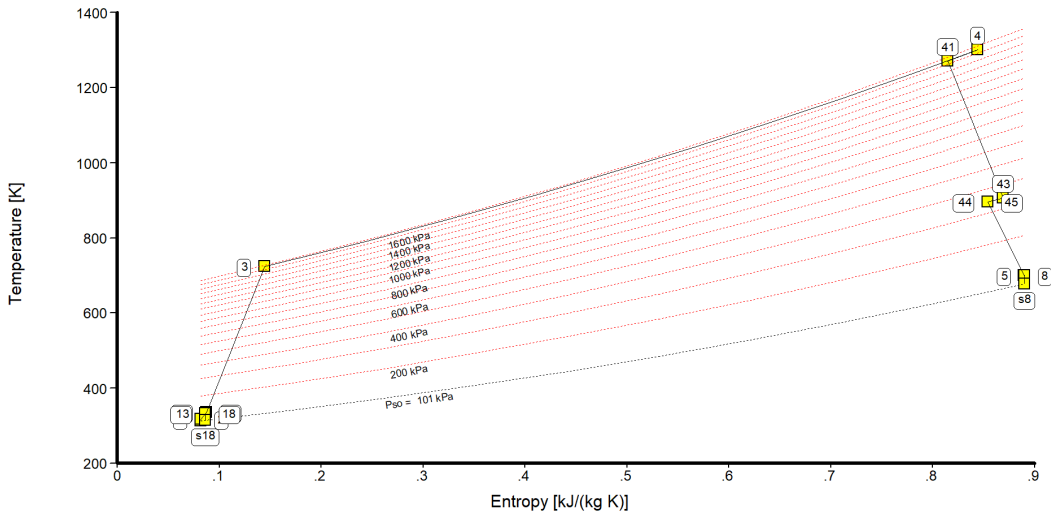


Figure 6: T-s diagram for the cruise condition;

4.2 Results and Proposed Specification

The proposed physical specification, as obtained via the design process outlined above, is summarised in table 2 as below. Table 2 also contains the assumed component efficiencies.

For each of the conditions considered, the required thrust, flight speed and critical engine temperatures are tabulated in table 3. The Gasturb analyses are included in appendix A of this report.

Table 2: Summary of engine specification at cruise;

Parameter		Value
Fan inlet conditions	T_o [K]	316.9
	P_o [kPa]	106.3
	\dot{m} [kg s^{-1}]	448.2
Bypass Ratio		13.0
TET [K]		1271.0
r_p	Fan	1.16
	Booster	1.20
	HP Compressor	13.0
	Overall Pressure Ratio	18.1
η_p	Fan	0.9020
	Booster	0.9025
	HP Turbine	0.8805
	LP Turbine	0.8864
η_{mech}	HP Shaft	1.0000
	LP Shaft	1.0000
η_s	HP Turbine	0.9000
	LP Turbine	0.9000

Table 3: Summary of design conditions and engine operating points;

Condition	Velocity choice	Working Engines	Mach Number	Required Thrust per Engine [kN]	TET [k]	T03 [k]	FPR	OPR
On-design	Max. range	6	0.267	44.6	1271	723	1.16	18.1
	Max. range	5	0.267	53.5	1445	782	1.19	21.4
Out of ground effect	Min. thrust	6	0.256	60.0	1600	831	1.21	24.2
	Min. thrust	5	0.256	71.9	1815	901	1.24	28.5

5 Turbomachinery Design

This section outlines the design method used to define the relevant engine dimensions and shaft speeds. This was based on the thermodynamic cycle for the engine discussed in the previous section and summarised in table 2. The dimensions calculated as per the procedure outlined in this section are shown in table 5 and a schematic of the engine is appended to this report as Appendix B. Figures 7 and 8 also show a flow chart summarising the design process. For more detailed commentary the reader is directed to the remainder of the section.

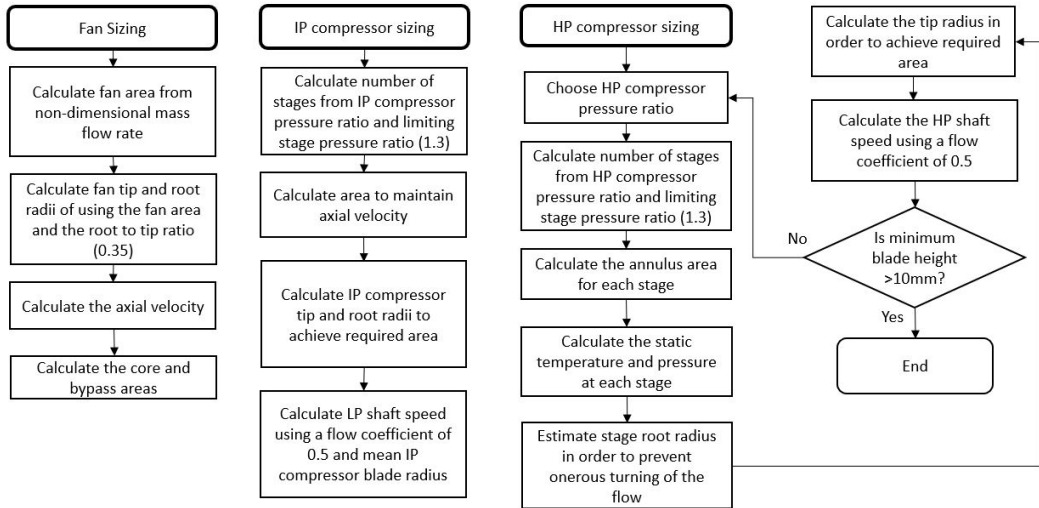


Figure 7: Summary flow charts of the design process for the fan, booster and HP compressor;

5.1 Fan

The inlet area was chosen to give a non dimensional mass flow rate of 0.85 times of that of a choked flow. For air with γ of 1.4 this implies a non-dimensional mass flow rate of 1.09 [Martinez-Botas and Davies, 2019b]. The fan area and Mach number could then be computed from the definition of the non-dimensional mass flow rate as given in equation 19.

$$\bar{m} = \frac{\dot{m}\sqrt{T_o c_p}}{AP_o} = \frac{\gamma}{\sqrt{\gamma - 1}} Ma \left(1 + \frac{\gamma - 1}{2} Ma^2\right)^{\frac{\gamma+1}{2(\gamma-1)}} \quad (19)$$

The values of the mass flow rate, \bar{m} , stagnation temperature, T_o , and stagnation pressure, P_o , at the inlet were all taken from the Gasturb output. These are tabulated in table 2. The tip and root radii of the fan could then be calculated from the fan area based on a root to tip ratio of 0.35, which is typical for engines of this type. The axial velocity was calculated at the fan inlet from the Mach number and the local speed of sound, which is a function of static temperature as shown in equation 20. As is discussed in the subsequent section, the cross sectional area of the core is chosen in order to maintain a constant axial velocity throughout the engine core,¹ through to the inlet of the exit nozzle.

$$a = \sqrt{\gamma RT} \quad (20)$$

The static conditions were calculated from the stagnation values using the Mach number at the inlet, and the core axial flow velocity (V_x) in subsequent stages. The static and stagnation conditions are

¹This does not necessarily need to be exactly the case in general, but it has been chosen here as suggested in Cumpsty and Heyes [2015] & Martinez-Botas and Davies [2019a] in order to simplify the calculations;

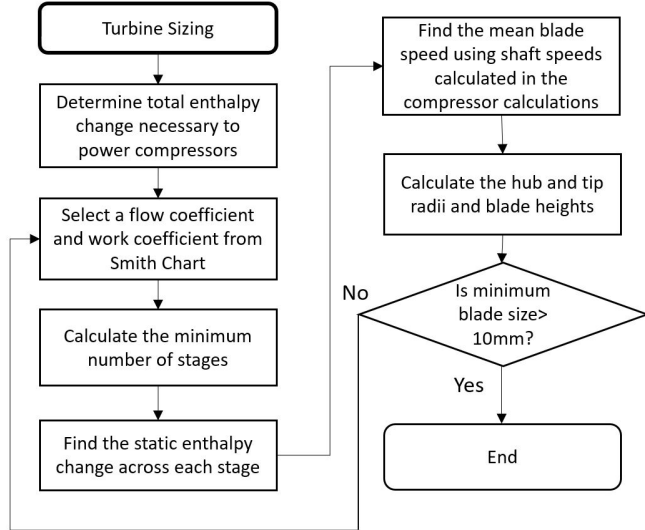


Figure 8: Summary flow chart of the design process for the HP and LP turbines;

related as per equations 21 and 22. The mass flow rate through the core was calculated from the bypass ratio which represents the ratio of the bypass mass flow to the core mass flow.

$$(T_o - T)C_p = \frac{1}{2}V_x^2 \quad (21)$$

$$\frac{P_o}{P} = \left(1 + \frac{\gamma - 1}{2}Ma^2\right)^{\frac{\gamma}{\gamma-1}} \quad (22)$$

In ‘conventional’ high bypass turbofans which operate at $Ma \approx 0.8$, the flow must be decelerated to the required engine-axial velocity of $Ma \approx 0.6$ to avoid excess compressibility effects of the flow at the blade tips. Therefore, these engines utilise diverging nozzles at the inlet. The aircraft considered in this report operates at relatively slow cruise velocities. Therefore, in order to simplify the calculations and utilise similar theory and turbomachinery components as a ‘conventional’ engine, the flow must be accelerated at the inlet and so a converging nozzle must be used. The calculated inlet diameter therefore was 2.0 m as shown by the drawing in B. It is appreciated that increasing the frontal area of the engine increases the bluff-body and nacelle drag, however in order to keep in line with standard turbomachinery components, it is deemed acceptable.

5.2 Booster Stage

The booster² is a single stage rotor-stator compressor (in general, there may be more than one stage however the pressure ratio required here is low enough to warrant a single stage. See table 2). In this two-shaft design, the booster sits on the low pressure shaft and runs at the same speed as the fan and low pressure turbine. The area of the booster stage was chosen such that the axial velocity remained constant throughout the core despite the variation in density due to compression. This relationship is illustrated in equation 23.

$$\dot{m} = \rho V_x A \quad (23)$$

Following the calculation of the annulus area, the blade length and positions were then chosen. In this case, in order to minimise turning of the airflow, the root of the booster blades were set to the

²otherwise termed the intermediate pressure compressor

Table 4: Shaft speeds;

Shaft	Speed [rad s ⁻¹]
Low pressure	1221.5
High pressure	1235.1

same radius as the root of the fan. It is desirable to minimise the turning of the air in order to prevent separation and thus keep losses in the core low. With the mean radius fixed, the angular velocity of the low pressure turbine was calculated from the flow coefficient defined as per equation 24 [Martinez-Botas and Davies, 2019a]. The speed is tabulated in table 4.

$$\phi_{booster} \equiv \frac{V_x}{U_m} = \frac{V_x}{\omega_{LP} R_m} = 0.5 \quad (24)$$

Where the mean blade radius is defined as,

$$R_m = \frac{1}{2}(R_t + R_r) \quad (25)$$

5.3 High Pressure Compressor

An 11 stage high pressure compressor was chosen in order to keep the pressure ratio across each stage below 1.3 as recommended in Martinez-Botas and Davies [2019a]. Each stage was designed so that the resulting pressure drop per stage is the same. This results in a pressure ratio per stage of 1.26. Combined with the polytropic efficiency given in table 2 and based on constant axial velocity, the relevant thermodynamic properties could be calculated. This then allowed the annulus area for each stage to be calculated using equation 23 in order to maintain a constant axial velocity. From this area distribution, the blade radii were chosen in order to align with the root of the booster and fan, limiting fluid turning.

Finally the speed of the high pressure shaft was calculated from the flow coefficient, taken as 0.5 as recommended in Martinez-Botas and Davies [2019a]. This relation is given in equation 26, and the speed is tabulated in table 4.

$$\phi_{HPC} \equiv \frac{V_x}{U_m} = \frac{V_x}{\omega_{HP} R_m} = 0.5 \quad (26)$$

Beyond the first stage, the root radius of the blades in the high pressure compressor reduced by 15 mm per stage. This was to maintain blade length above 10 mm at the compressor exit, where the annulus area reduces due to higher air density.

5.4 Turbines

The inlet conditions for the high pressure turbine was defined by the turbine entry temperature given in table 2 and, assuming no pressure drop across the combustor, a pressure equal to that at the exit of the compressor stages.

The flow coefficient for the high pressure turbine was taken to be 0.8. This exceeds the recommended values in Cumpsty and Heyes [2015] but is required in order to prevent overly sharp turns in the flow. To maintain a smooth transition between the high and low pressure turbines, the flow coefficient for the low pressure turbine was taken at the lower limit as suggested by Cumpsty and Heyes [2015] of 0.7. The isentropic efficiency of the turbines was given by Gasturb (see table 2) which then allows the work coefficient to be determined from the Smith chart (figure 9). The stagnation temperature change per stage is then calculated from the definition of the work coefficient as shown in equation 27.

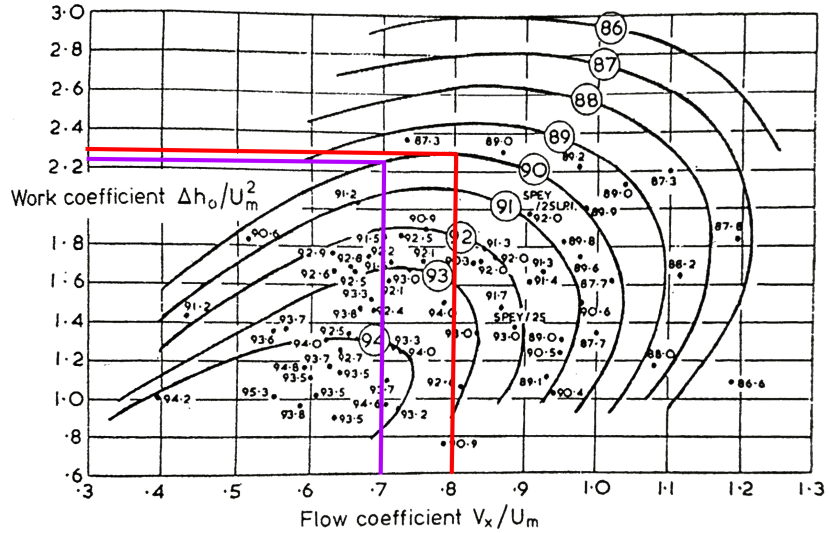


Figure 9: ‘Smith’ chart. Variation in measured stage efficiency with stage loading and flow coefficient for axial-flow turbines [Cumpsty and Heyes, 2015]. The low and high pressure stages are shown in purple and red respectively.

$$\psi = \frac{\Delta h_o}{U_o^2} = \frac{C_p \Delta T_o}{U_o} = f(\phi, \eta_s) \quad (27)$$

The total stagnation temperature change across the high and low pressure turbines respectively is calculated from the enthalpy change across the compressor stages on the relevant shaft. This is shown in equations 28 & 29. The number of stages suggested by the overall and per-stage stagnation temperature changes was rounded up, giving a lower per-stage stagnation temperature reduction in each case than suggested by the Smith chart.

$$\Delta T_{HPT} = -\frac{c_{p,air} \Delta T_{HPC}}{\eta_{mech,HPC} c_{p,soot}} \quad (28)$$

$$\Delta T_{LPT} = -\frac{\dot{m}_{fan} c_{p,air} \Delta T_{fan} + \dot{m}_{core} c_{p,air} \Delta T_{booster}}{\dot{m}_{LPT} \eta_{mech,LPC} c_{p,soot}} \quad (29)$$

From the total required enthalpy changes, and the possible enthalpy change per stage calculated from the work coefficients, the number of turbine stages can be calculated.

Given that the shaft speeds are fixed by the compressor design, equations 24 & 26 in the case of the compressor define the mean blade radius. Using calculated thermodynamic quantities and equation 23, the area for each stage can be calculated and therefore the tip and root radius is defined around the mean radius.

5.5 Nozzle outlets

The nozzle outlet conditions were calculated based on the assumption that the flow was fully expanded (that being that the static temperature at both bypass and core nozzle exits were ambient). The areas could be calculated from the non-dimensional mass flow rates in a manner similar to what has been shown previously (see equation 19). From this, the effective diameter of the nozzle could be ascertained considering the inner radius of the nozzle non-zero. The calculated area for the core and bypass nozzles were 0.33 m^2 and 1.22 m^2 respectively. This corresponded to exit diameters of 0.6 m and 1.3 m .

Table 5: Key calculation parameters;

Stage	ρ [kg m ⁻³]	T_o [k]	P_o [kPa]	r_p ³	Area [m ⁻²]	Mach	a [ms ⁻¹]	η_p	R_r [mm]	R_t [mm]	R_a [mm]	Blade Length [mm]
Fan Inlet	1.0	316.9	106.3	-	2.1843	0.61	344.2	-	311.6	890.1	600.8	578.6
Booster Inlet	1.1	332.2	123.3	1.16	0.1398	0.59	353.0	0.902	311.6	376.2	343.9	64.7
HP Compressor Inlet	1.2	351.9	148.0	1.20	0.1222	0.58	364.1	0.903	311.6	368.7	340.1	57.2
HPC S2 Inlet	1.5	378.1	186.8	1.26	0.1028	0.56	378.3	0.928	296.6	347.4	322.0	50.8
HPC S3 Inlet	1.8	406.2	235.9	1.26	0.0865	0.53	392.9	0.928	281.6	326.8	304.2	45.3
HPC S24 Inlet	2.1	436.5	297.8	1.26	0.0729	0.51	408.1	0.928	266.6	307.0	286.8	40.5
HPC S5 Inlet	2.5	468.9	376.0	1.26	0.0615	0.50	423.8	0.928	251.6	287.8	269.7	36.3
HPC S6 Inlet	2.9	503.8	474.8	1.26	0.0519	0.48	440.0	0.928	236.6	269.2	252.9	32.7
HPC S7 Inlet	3.5	541.3	599.5	1.26	0.0438	0.46	456.8	0.928	221.6	251.1	236.3	29.5
HPC S8 Inlet	4.1	581.6	756.9	1.26	0.0370	0.44	474.2	0.928	206.6	233.3	219.9	26.8
HPC S9 Inlet	4.9	624.9	955.7	1.26	0.0313	0.43	492.2	0.928	191.6	216.0	203.8	24.4
HPC S10 Inlet	5.8	671.4	1206.6	1.26	0.0264	0.41	510.8	0.928	176.6	199.0	187.8	22.4
HPC S11 Inlet	6.8	721.4	1523.5	1.26	0.0224	0.40	530.1	0.928	161.6	182.3	171.9	20.7
Combuster Inlet	8.0	775.1	1923.6	1.26	0.0189	0.38	550.1	0.928	146.6	165.8	156.2	19.3
HP Turbine Inlet	5.0	1271.0	1923.6	1.00	0.0302	0.30	708.4	1.000	201.3	223.9	212.6	22.6
HPT S2 Inlet	3.5	1157.1	1211.7	0.63	0.0438	0.31	675.3	0.881	213.9	244.3	229.1	30.4
LP Turbine Inlet	2.5	1062.9	797.9	0.66	0.0614	0.32	646.7	0.881	225.8	265.5	245.6	39.8
LPT S2 Inlet	1.7	968.7	506.9	0.64	0.0885	0.34	616.8	0.886	233.8	287.8	260.8	54.0
LPT S3 Inlet	1.1	874.5	307.4	0.61	0.1326	0.36	585.3	0.886	241.8	317.2	279.5	75.5
LPT S4 Inlet	0.7	780.3	176.1	0.57	0.2081	0.38	552.0	0.886	249.8	358.6	304.2	108.9

³Pressure ratio compared with previous stage;

6 Blade Geometry

Flow angles (α and β) were calculated for each stage at the mean, tip and root radius using the thermodynamic properties calculated and updated as shown in table 5. The number of blades, n , chord length, c , thickness, h , and pitch, s , were also calculated at mean radius for each stage. A number of best practice constraints were observed when choosing geometry for the compressor and turbine stages [Martinez-Botas and Davies, 2019b]. These constraints are summarised in table 6.

Table 6: Blade constraints;

Quantity	Bounds	Applicability
DF	< 0.5	Compressors and Turbines
t/c	0.75 – 1.5	Compressors and Turbines
s/c	0.6 – 1.5	Compressors and Turbines
z_w	< 0.8	HP Turbine
z_w	< 1	LP Turbine

The Lieblen diffusion factor, DF , is used to predict the pressure loss incurred due to turning and acceleration of the flow. It can be expressed as per equation 30 [Martinez-Botas and Davies, 2019d], where the subscripts 2 and 3 represent locations up and downstream of the rotor stage.

$$DF = \left(1 - \frac{\cos(\alpha_2)}{\cos(\alpha_3)}\right) + \frac{\cos(\alpha_2)}{2c/s} (\tan(\alpha_3) - \tan(\alpha_2)) \quad (30)$$

z_w is the Zweifel coefficient and is defined for a turbine rotor as per equation 31.

$$z_w = \frac{2s}{c} \cos^2(\alpha_3) (\tan(\alpha_2) - \tan(\alpha_3)) \quad (31)$$

The required turning of the flow by the rotor stage was calculated by the Euler turbo-machinery equation as per equation 32 [Cumpsty and Heyes, 2015]. This was based on the necessary temperature change at each stage as tabulated in 5. Once α_2 & α_3 were chosen to achieve the required enthalpy change across the rotor DF and z_w were computed in order to ensure that they were within the limits set out in table 6.

$$c_p \Delta T_{0,stage} = U v_x (\tan(\alpha_3) - \tan(\alpha_2)) = U v_x (\tan(\beta_2) - \tan(\beta_3)) \quad (32)$$

The turning of the flow by the stator was a design choice that defined the flow direction at entry to the next rotor stage. This design choice was made in order to adhere to the constraints shown in table 6. The mean blade angles and number of blades for each stage is shown in table 7. The number of blades at each stage was calculated as per equation 33.

$$n = \frac{2\pi R_m}{s} \quad (33)$$

Up until now, only the mean radius of the blade has been considered and designed. If the axial velocity through the turbine is assumed constant along the radius of the blade, the product of the tangential absolute velocity and radius must also be constant as per equation 34.

$$R_m c_{\theta,m} = R_t c_{\theta,t} = R_r c_{\theta,r} = constant \quad (34)$$

Where c_θ is the tangential axial velocity⁴, and the subscripts r , m and t refer to the root, mean and tip positions. In addition to the inverse scaling of tangential velocity with radius as shown above, the relative velocity is also affected by the blade speed which must be scaled proportionally with radius as in equation 35.

⁴Not to be confused with the chord length, c ;

$$\frac{U_m}{R_m} = \frac{U_t}{R_t} = \frac{U_r}{R_r} = \text{constant} \quad (35)$$

This allows the flow angles at the tip and root of the blade to be calculated from the values found at the mean radius. Blade sketches including flow angles are shown for mean, tip and root radius for the final HP compressor stage and final HP turbine stage in figure 10. In all cases, the aspect ratio and pitch-to-chord ratios are fixed at unity.

Table 7: Blade angles, number of blades, Zweifel coefficients and diffusion factors. All at mean radius with angles in degrees;

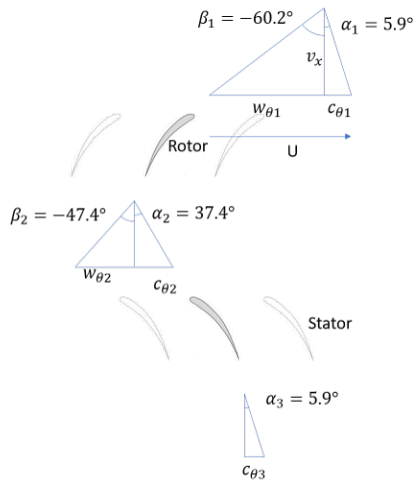
Stage	s/c	n	h/c	$\alpha_{1,m}$	$\alpha_{2,m}$	$\alpha_{3,m}$	$\beta_{1,m}$	$\beta_{2,m}$	$\beta_{3,m}$	D	Z_w
Fan	1.0	28	1.0	0.00	5.68	0.0	-74.0	-73.6	-	0.0448	-
Booster	1.0	35	1.0	0.00	12.7	5.45	-63.4	-60.6	-	0.0874	-
HPC Stage 1	1.0	37	1.0	5.45	21.5	5.45	-62.3	-58.1	-	0.0787	-
HPC S2	1.0	39	1.0	5.45	22.6	5.45	-62.3	-57.7	-	0.0814	-
HPC S3	1.0	40	1.0	5.45	23.7	5.45	-62.3	-57.3	-	0.0840	-
HPC S4	1.0	40	1.0	5.45	25.0	5.45	-62.3	-56.9	-	0.0862	-
HPC S5	1.0	40	1.0	5.45	26.2	5.45	-62.3	-56.4	-	0.0881	-
HPC S6	1.0	40	1.0	5.45	27.6	5.45	-62.3	-55.9	-	0.0895	-
HPC S7	1.0	40	1.0	5.45	29.0	5.45	-62.3	-55.3	-	0.0903	-
HPC S8	1.0	40	1.0	5.45	30.5	5.45	-62.3	-54.7	-	0.0904	-
HPC S9	1.0	40	1.0	5.45	32.0	5.45	-62.3	-54.0	-	0.0898	-
HPC S10	1.0	40	1.0	5.45	33.6	5.45	-62.3	-53.2	-	0.0881	-
HPC S11	1.0	40	1.0	5.45	35.3	5.45	-62.3	-52.3	-	0.0854	-
HPT Stage 1	1.0	40	1.0	13.4	-66.8	13.4	-	-47.2	56.1	-	0.795
HPT S2	1.0	42	1.0	13.4	-62.1	13.4	-	-32.5	56.1	-	0.621
LPT Stage 1	1.0	44	1.0	5.45	-60.4	5.45	-	-18.5	56.7	-	0.603
LPT S2	1.0	46	1.0	5.45	-60.4	5.45	-	-18.5	56.7	-	0.603
LPT S3	1.0	48	1.0	5.45	-60.4	5.45	-	-18.5	56.7	-	0.603
LPT S4	1.0	50	1.0	5.45	-60.4	5.45	-	-18.5	56.7	-	0.603

Table 7 presents the diffusion factors and diffusion factors and the Zweifel coefficients at mean radius. These remain within acceptable design limits for all blades. Blade angles for the different blade radii are shown in 10, for the final stage HP compressor and the final stage HP turbine. The Zweifel coefficients and diffusion factors at the three radii are also presented in table 8. Again, these all remain within acceptable limits.

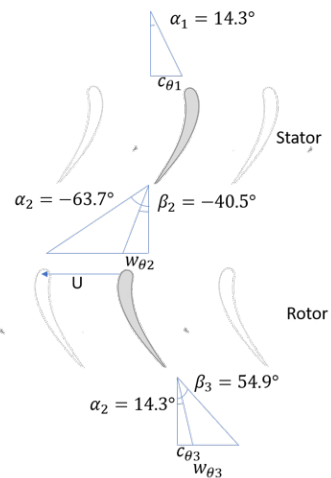
Table 8: Zweifel coefficients and diffusion factors for the final stages of the HPC and HPT at the root tip and mean radii;

Parameter	Radius	Value
<i>DF</i> for	root	0.0854
HPC S11	mean	0.0789
	tip	0.0902
<i>z_w</i> for	root	0.621
HPT S2	mean	0.597
	tip	0.643

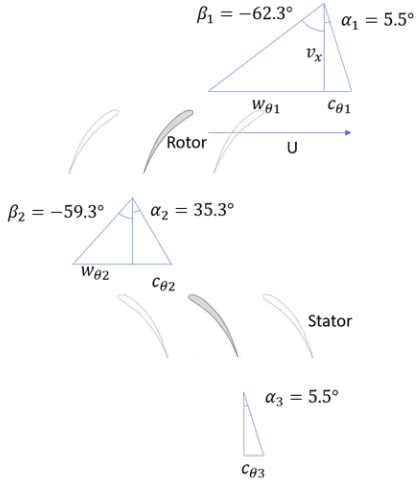
Final Stage HP Compressor Root Radius



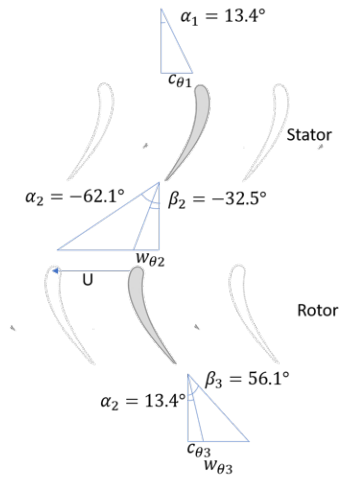
Final Stage HP Turbine Root Radius



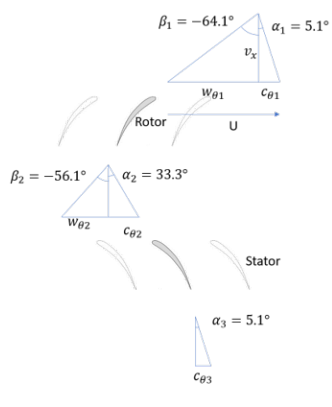
Final Stage HP Compressor Mean Radius



Final Stage HP Turbine Mean Radius



Final Stage HP Compressor Tip Radius



Final Stage HP Turbine Tip Radius

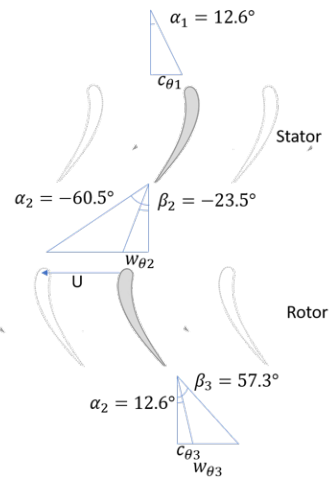


Figure 10: Blade sketches;

7 HPT Disc Stresses

In an aero turbine, the disc is the structural component on which the turbine blades are mounted as shown in Figure 11. It is important to analyse the stress distributions throughout the discs to ensure that they do not fail during operation, or are not over-specified (i.e large safety factors increase weight which is undesirable). In practice, finite element methods are utilised due to the complex nature of the blade and disc geometries. However, analytical estimates can be obtained if certain assumptions are made. This section will outline this process and give the estimated stress distributions and safety factors. Broadly, the calculations presented here follow the methods outlined in Martinez-Botas and Davies [2019c]. The disc and blade material is Inconel 718, a heat resistant superalloy with a density of 8193.3 kg m^{-3} as given (along with other material properties) by the manufacturer datasheet [Special Metals Corporation, 2007].

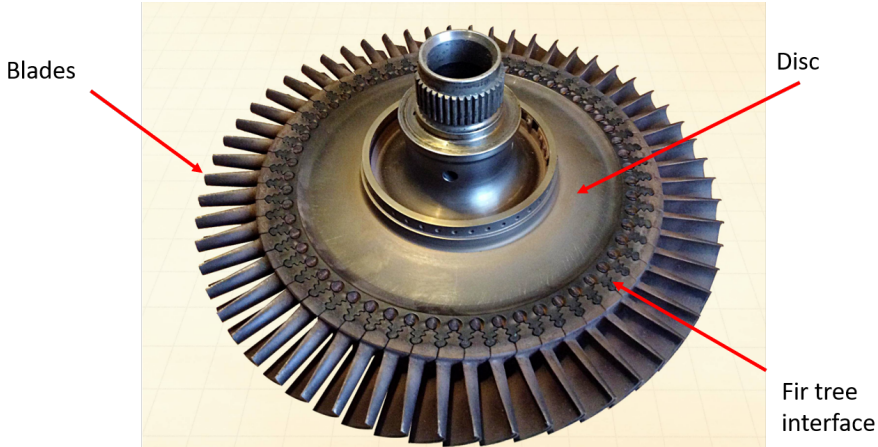


Figure 11: Image of turbine rotor stage including disc and blades

The first assumption made is that the disc is under plane stress conditions, meaning that the blades are exerting no axial force on the disc. This implies that the blades are only providing a net centrifugal force on the rim of the disc which in turn contributes to both radial and circumferential (hoop) stresses. The centrifugal force generated by each blade can be calculated by considering it as a point mass rotating at its mean radius around the disc centre. From this, the force on the rim can be calculated as per equation 36.

$$F_{rim} = m_b \omega^2 R_m \quad (36)$$

Where m_b is the blade mass and ω is the angular velocity of the high pressure shaft. In order to calculate the mass of each blade, the volume and density are needed. For the sake of this estimate, the volume of each blade was taken as the product of the chord length, mean thickness and the blade length. It is then assumed that only 10% of the blade volume is solid and that the rest represents cooling channels and empty space. As shown previously in Table 4, the high pressure shaft rotational speed is 1235 rad s^{-1} . The pertinent values for each HP turbine rotor stage including the calculated rim force can be found in Table 9.

Table 9: HPT blade data;

Stage	c [mm]	t [mm]	L [mm]	m_b [kg]	F_{rim} [kN]	n
1	29.8	29.8	20.3	0.0168	6.02	40
2	45.9	45.9	27.3	0.0471	17.1	42

With the centrifugal force from the blades and the number of blades, the stresses through the discs

can now be computed. In order to do this analytically, some assumptions have been made and are listed below.

- The disc is rotating at a constant speed
- The temperature, Poissons ratio (ν) and elastic modulus (E) are uniform and independent of radius
- The stress distribution is elastic
- The disc is a constant thickness, t_d

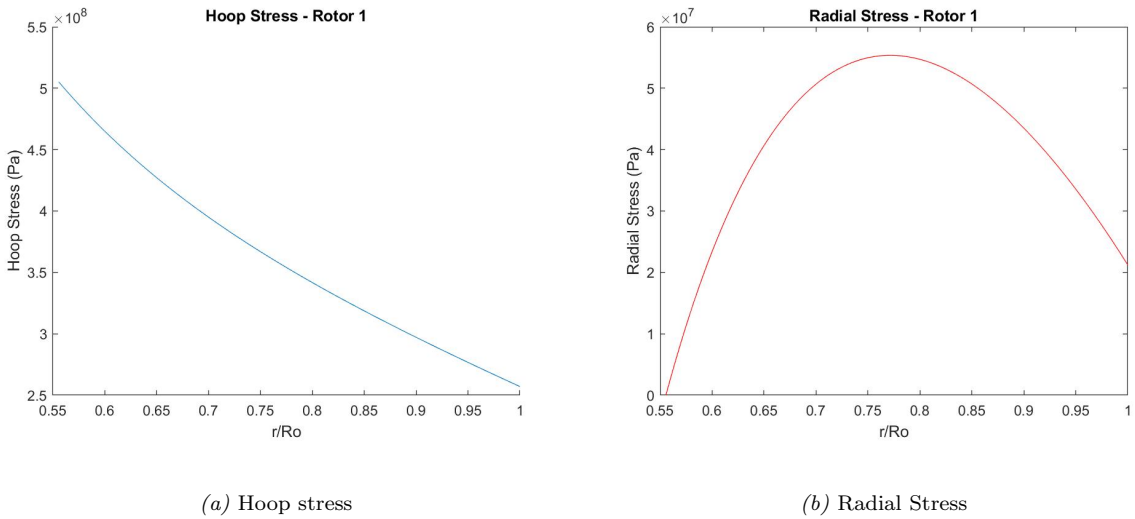
By considering a volume element within the disc, equating it's tractions and integrating, a force balance can be obtained for the disc. Using this in conjunction with Hooke's law and appropriate boundary conditions gives equations 37 & 38 for the radial and hoop stresses at a given radius R respectively.

$$\sigma_R = \frac{3 + \nu}{8} \rho \omega^2 \left(R_i^2 + R_o^2 - \left(\frac{R_i R_o}{R} \right)^2 - R^2 \right) + \frac{n F_{rim} R_o}{2\pi t_d (R_o^2 - R_i^2)} \left[1 - \left(\frac{R_i}{R} \right)^2 \right] \quad (37)$$

$$\sigma_\theta = \frac{3 + \nu}{8} \rho \omega^2 \left(R_i^2 + R_o^2 + \left(\frac{R_i R_o}{R} \right)^2 - \frac{1 + 3\nu}{3 + \nu} R^2 \right) + \frac{n F_{rim} R_o}{2\pi t_d (R_o^2 - R_i^2)} \left[1 + \left(\frac{R_i}{R} \right)^2 \right] \quad (38)$$

Where σ_r represents the radial stress and σ_θ represents the hoop stress. Equations 37 and 38 can be solved for varying radius (R) along the disc to determine the stress distribution throughout. Using the Tresca yield criterion and the yield stress of the material, a safety factor against yielding can be determined. In fact, one can work backwards from this point; i.e by setting a desired safety factor, it is possible to determine the maximum allowable stress in the blade, adjusting the variables in equations 37 and 38 where appropriate. For the engine considered in this report, a safety factor against yield between 1.1 and 1.2 was chosen. This was to allow sufficient contingency against failure whilst keeping weight to a minimum. As the blade radii had been set in a previous section, the disc thickness, t_d was varied to keep safety factors at the desired level.

The calculated stresses throughout both HPT rotor stages are presented in Figures 12 and 13.



(a) Hoop stress

(b) Radial Stress

Figure 12: Stress distribution through the first HP turbine rotor disc

The above figures show that in both stages, the maximum stress according to a Tresca criterion is the hoop stress at the disc root at 500 and 750 MPa for stages 1 and 2 respectively. The yield stress of IN718 is a function of temperature, and thus will be different for each turbine stage. The flow

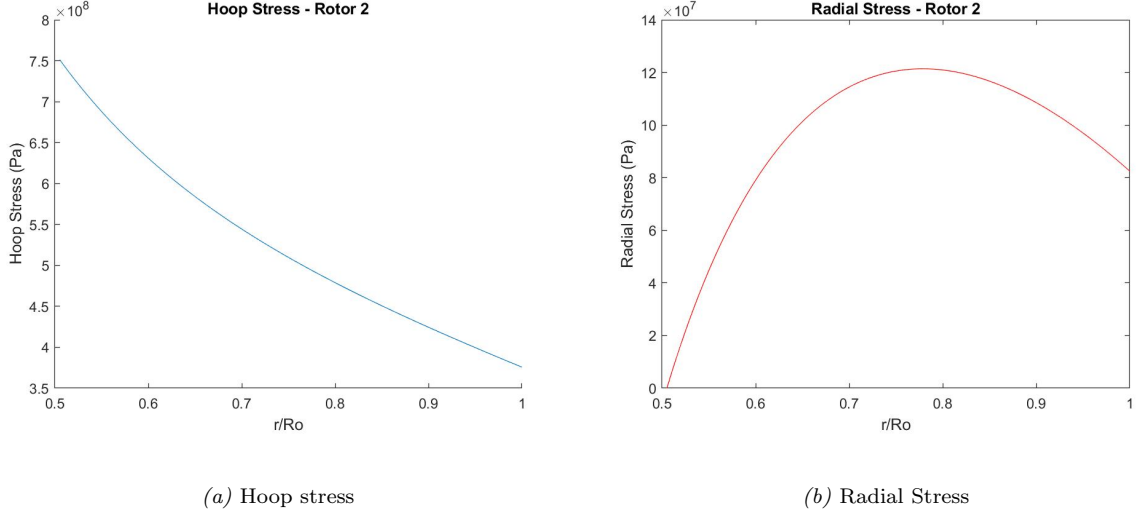


Figure 13: Stress distribution through the second HP turbine rotor disc

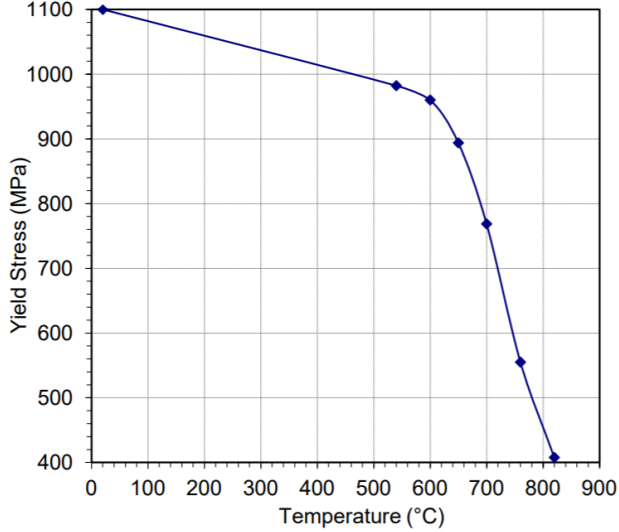


Figure 14: IN718 yield stress as a function of temperature

temperatures through the stages are tabulated in table 5. However, that considers the flow itself and not the blades/discs where significant cooling takes place. It is estimated by Yahya [2010] that blade temperature can be reduced by 200-300 K through air cooling. In this analysis, the assumption was made that there was no temperature gradient through the disc meaning that the disc must be at the same temperature as the blade. The amount of cooling in terms of temperature was taken to be 250 K for each stage. The yield stress values at the different temperatures were then taken from the graph in Figure 14 [Martinez-Botas and Davies, 2019c].

With the yield stresses now determined, the disc thickness was varied in order to achieve the desired safety factor of between 1.1 and 1.2. Table 10 shows the results of this where $\tilde{\sigma}$ is the Tresca stress which is defined as,

$$\tilde{\sigma} = \text{Max}[\sigma_\theta - \sigma_r; \sigma_\theta - \sigma_z; \sigma_z - \sigma_r] \quad (39)$$

Table 10: HPT Safety factors;

Stage	T_{flow} [K]	T_{disk} [K]	σ_{yield} [MPa]	t_d [mm]	$\tilde{\sigma}$ [MPa]	Safety Factor
1	1271	1021	601	10	505	1.19
2	1136	863	897	7	751	1.20

8 Conclusions & Further Work

The calculations detailed in this report demonstrate that it is possible to design a GEV capable of flying above the waves expected in the north Atlantic. The engine is capable of flying out of the ground effect should it be necessary without exceeding the maximum engine temperatures. The engine is a two-spool, high-bypass turbofan engine with a BPR of 13.0. At cruise it operates an OPR of 18.1, a FPR of 1.16 and turbine entry and compressor exit temperatures of 1271 K and 723 K respectively. The engines are capable of powering the craft both in and out of the ground effect when one engine is damaged.

Overall, the engine designed for the craft in this example consumes more fuel on a journey to New York than an aircraft of comparable size, such as the A380. Despite the lower fuel consumption per hour, this GEV consumes a total of 167 tonnes of fuel compared to an A380's 97 tonnes of fuel. This result is likely to be because the L/D ratios used herein were 14 and 9 for the in and out of ground effect cases respectively. This is much lower than would be expected on a modern airliner as the airframe chosen was designed in the 1970s and did not benefit from more modern computational design techniques. Modern airliners are capable of L/D ratios of approximately 20, whereas equivalent airliners in the 70s had ratios closer to 13. If a similar gain (c.50%) in L/D ratio between the in and out of ground effect cases could be achieved on a more modern airframe it is expected that a far more favorable result could be obtained. Examples of more contemporary GEVs include the Boeing Pelican which can achieve L/D ratios of up to 45 when in ground effect [Rowdon and Hoisington, 2004].

The craft would complete its journey from Portsmouth to New York in 17 hours, this is within the design aim and is deemed to be acceptable if the craft were a more efficient alternative.

The height of the waves expected in the North Atlantic also limit the benefits than can be achieved from the ground effect. The cruise height considered herein is far greater than the Ekranoplan's original 5 m resulting in a higher induced drag factor and lower L/D than could be achieved in lower wave heights, such as those in the Caspian Sea.

A number of simplifications were implemented in the design of this engine, and ideal CDF and FEA analysis techniques would be implemented in order to further refine the design of the blades. Many of the best practices implemented herein were developed in the design of engines flying at much greater velocities at much higher altitudes than a GEV. This has led to some unusual design choices, such as the converging nozzle at the fan inlet. The choice of axial velocity could be revised in order to remove the need for this nozzle in future iterations of this design. No consideration has been given to fatigue or creep in the design of the disk.

9 References

- Focusing on environmental pressures from long-distance transport. Technical report 7, European Environment Agency, 2014.
- N. Cumpsty and A. Heyes. *Jet Propulsion: A simple guide to the aerodynamics and thermodynamic design and performance of jet engines*. Cambridge University Press, New York, 3rd edition, 2015. ISBN 9780521541442.
- Y. Lin and S. Dong. Wave energy assessment based on trivariate distribution of significant wave height, mean period and direction. *Applied Ocean Research*, 87:47–63, 2019.
- P. Mantle. Induced drag of wings in ground effect. *The Aeronautical Journal*, 120(1234):1867–1890, 2016.
- R. Martinez-Botas and C. Davies. Aircraft engine technology: Coursework task 2, 2019a. Department of Mechanical Engineering, Imperial College London.
- R. Martinez-Botas and C. Davies. Aircraft engine technology: Course notes, 2019b. Department of Mechanical Engineering, Imperial College London.
- R. Martinez-Botas and C. Davies. Aircraft engine technology: Stress analysis of blades and discs, 2019c. Department of Mechanical Engineering, Imperial College London.
- R. Martinez-Botas and C. Davies. Aircraft engine technology: Turbomachinery, 2019d. Department of Mechanical Engineering, Imperial College London.
- B. K. Rowdon and Z. C. Hoisington. Characteristics of an ultra-large, land-based wind-in-ground effect aircraft. pages 228–36, Sydney, 2004. Proceedings of Pacific 2004 International Maritime Conference.
- SNAME, 2008. Technical and Research Bulletin 5-5A: Guidelines for site specific assessment of mobile jack-up units. Standard, Society of Naval Architects and Marine Engineers, New Jersey, US, August 2008.
- Special Metals Corporation, 2007. Inconel alloy 718. Datasheet.
- S. M Yahya. *Turbines, Compressors and Fans*. McGraw-Hill Education, New York, US, 4th edition, 2010. ISBN 9780070707023.
- L. Yun, A. Bliault, and J. Doo. *WIG Craft and Ekranoplan: Ground Effect Craft Technology*. Springer, New York, 2010. ISBN 9781441900418.
- D Zhang and D. Xu. A new maximum entropy probability function for the surface elevation of nonlinear sea waves. *China Ocean Engineering*, 19(4):637–646, 2005.

A Gasturb Outputs

A.1 On-Design Cruise Condition

Geared Fan Alt= 13m / Mn=0.267 Mil Std 210A Hot Day

Station	W	T	P	WRstd	FN	=	44.57
amb		312.46	101.164		TSFC	=	10.1576
2	448.163	316.89	106.297	448.000	WF	=	0.4528
13	416.151	332.09	123.305	367.121	s NOX	=	0.5252
21	32.012	316.90	106.308	31.997	Core Eff	=	0.3958
24	32.012	335.67	127.569	27.442	Prop Eff	=	0.6559
25	32.012	335.67	127.569	27.442	BPR	=	13.0000
3	32.012	723.27	1658.399	3.099	P2/P1	=	1.0000
31	27.850	723.27	1658.399		P3/P2	=	15.60
4	28.303	1300.00	1658.399	3.673	P5/P2	=	1.0792
41	29.903	1271.00	1658.399	3.837	P16/P13	=	1.00000
43	29.903	905.89	340.015		P16/P6	=	1.07488
44	31.824	895.32	340.015		P16/P2	=	1.16000
45	31.824	895.32	340.015	16.717	P6/P5	=	1.00000
49	31.824	699.50	114.715		A8	=	0.29682
5	32.464	699.97	114.715	44.692	A18	=	2.05950
8	32.464	699.97	114.715	44.692	XM8	=	0.43391
18	416.151	332.09	123.305	367.122	XM18	=	0.53956
					CD8	=	0.94250
Efficiencies:	isentr	polytr	RNI	P/P	CD18	=	0.93939
Outer LPC	0.9000	0.9020	0.894	1.160	PWX	=	50.00000
Inner LPC	0.9000	0.9672	0.894	1.000	V18/V8,id=	=	0.85939
IP Compressor	0.9000	0.9025	0.894	1.200	WBLD/W21	=	0.00000
HP Compressor	0.9000	0.9280	0.973	13.000	WBLD/W25	=	0.00000
Burner	1.0000			1.000	Loading %	=	100.00
HP Turbine	0.9000	0.8805	1.371	4.877	e444 th	=	0.87001
LP Turbine	0.9000	0.8864	0.501	2.964	WHcl/W25	=	0.06000
HP Spool mech	1.0000	Nominal Spd		37000	WLcl/W25	=	0.02000
LP Spool mech	1.0000	Nominal Spd		12800			
Bleed Air:	PBld = 1658.39	TBld =	723.3		ZWBld	=	0.00000
hum [%]	war0	FHV	Fuel				
0.0	0.00000	43.124	Generic				

A.2 Cruise Condition, Five Engines

Alt= 13m / Mn=0.267 Mil Std 210A Hot Day , Rel Speed=1.100

Station	W	T	P	WRstd	FN	=	53.46
amb		312.46	101.164		TSFC	=	11.4265
2	472.653	316.89	106.297	472.481	WF	=	0.6109
13	438.141	336.46	125.948	380.886	s NOX	=	0.7538
21	34.511	316.90	106.309	34.495	Core Eff	=	0.4049
24	34.511	338.16	126.518	29.942	Prop Eff	=	0.6264
25	34.511	338.16	126.518	29.942	BPR	=	12.6956
3	34.511	782.27	1916.078	3.007	P2/P1	=	1.0000
31	30.025	782.27	1916.078		P3/P2	=	18.03
4	30.636	1479.51	1916.078	3.671	P5/P2	=	1.1190
41	32.361	1445.00	1916.078	3.832	P16/P13	=	1.00000
43	32.361	1037.22	391.665		P16/P6	=	1.05890
44	34.432	1022.70	391.665		P16/P2	=	1.18487
45	34.432	1022.70	391.665	16.781	P6/P5	=	1.00000
49	34.432	786.11	118.943		A8	=	0.29682
5	35.122	786.03	118.943	49.416	A18	=	2.05950
8	35.122	786.03	118.943	49.416	XM8	=	0.49545
18	438.141	336.46	125.948	380.886	XM18	=	0.56863
					CD8	=	0.94603
Efficiencies:	isentr	polytr	RNI	P/P	CD18	=	0.94180
Outer LPC	0.8017	0.8063	0.894	1.185	PWX	=	50.00000
Inner LPC	0.8017	0.8477	0.894	1.000	V18/V8,id=	=	0.75724
IP Compressor	0.7577	0.7635	0.894	1.190	WBLD/W21	=	0.00000
HP Compressor	0.8528	0.8955	0.953	15.145	WBLD/W25	=	0.00000
Burner	1.0000			1.000	Loading %	=	68.29
HP Turbine	0.9029	0.8846	1.283	4.892	e444 th	=	0.87479
LP Turbine	0.8996	0.8850	0.463	3.293	WHcl/W25	=	0.06000
HP Spool mech	1.0000	Speed		40696.12	WLcl/W25	=	0.02000
LP Spool mech	1.0000	Speed		14509.88			
Bleed Air:	PBld = 1916.08	TBld = 782.3			ZWBld	=	0.00000
hum [%]	war0	FHV	Fuel				
0.0	0.00000	43.124	Generic				

A.3 Out of Ground Effect, Minimum Thrust, Six Engines

Alt= 300m / Mn=0.256 Mil Std 210A Hot Day , Rel Speed=1.190

Station	W	T	P	WRstd	FN	=	60.13
amb		310.48	97.773		TSFC	=	12.2783
2	473.907	314.53	102.328	490.274	WF	=	0.7383
13	439.012	337.89	123.571	389.813	s NOX	=	0.9930
21	34.895	314.55	102.341	36.096	Core Eff	=	0.4080
24	34.895	336.86	118.195	32.344	Prop Eff	=	0.5883
25	34.895	336.86	118.195	32.344	BPR	=	12.5810
3	34.895	830.64	2048.602	2.930	P2/P1	=	1.0000
31	30.359	830.64	2048.602		P3/P2	=	20.02
4	31.097	1639.42	2048.602	3.669	P5/P2	=	1.1597
41	32.842	1600.00	2048.602	3.828	P16/P13	=	1.00000
43	32.842	1156.07	418.773		P16/P6	=	1.04132
44	34.935	1137.73	418.773		P16/P2	=	1.20760
45	34.935	1137.73	418.773	16.796	P6/P5	=	1.00000
49	34.935	867.63	118.668		A8	=	0.29682
5	35.633	866.94	118.668	52.774	A18	=	2.05950
8	35.633	866.94	118.668	52.774	XM8	=	0.54455
18	439.012	337.89	123.571	389.813	XM18	=	0.58846
					CD8	=	0.94909
Efficiencies:	isentr	polytr	RNI	P/P	CD18	=	0.94349
Outer LPC	0.7430	0.7497	0.871	1.208	PWX	=	50.00000
Inner LPC	0.7430	0.7474	0.871	1.000	V18/V8,id=	=	0.68365
IP Compressor	0.5903	0.5986	0.871	1.155	WBLD/W21	=	0.00000
HP Compressor	0.8147	0.8700	0.896	17.332	WBLD/W25	=	0.00000
Burner	1.0000			1.000	Loading %	=	52.10
HP Turbine	0.9043	0.8866	1.159	4.892	e444 th	=	0.87771
LP Turbine	0.8974	0.8819	0.415	3.529	WHcl/W25	=	0.06000
HP Spool mech	1.0000	Speed		44038.25	WLcl/W25	=	0.02000
LP Spool mech	1.0000	Speed		15638.93			
Bleed Air:	PBld = 2048.60	TBld = 830.6			ZWBld	=	0.00000
hum [%]	war0	FHV	Fuel				
0.0	0.00000	43.124	Generic				

A.4 Out of Ground Effect, Minimum Thrust, Five Engines

Alt= 300m / Mn=0.256 Mil Std 210A Hot Day , Rel Speed=1.324

Station	W	T	P	WRstd	FN	=	71.91
amb		310.48	97.773		TSFC	=	13.6154
2	499.136	314.53	102.328	516.375	WF	=	0.9791
13	462.172	343.83	126.915	403.060	s NOX	=	1.5087
21	36.964	314.55	102.343	38.237	Core Eff	=	0.4148
24	36.909	338.62	114.408	35.435	Prop Eff	=	0.5577
25	37.364	338.62	114.408	35.872	BPR	=	12.5031
3	37.364	901.14	2354.399	2.844	P2/P1	=	1.0000
31	32.507	901.14	2354.399		P3/P2	=	23.01
4	33.486	1861.51	2354.399	3.663	P5/P2	=	1.2217
41	35.354	1815.38	2354.399	3.819	P16/P13	=	1.00000
43	35.354	1323.16	481.015		P16/P6	=	1.01517
44	37.596	1299.88	481.015		P16/P2	=	1.24028
45	37.596	1299.88	481.015	16.820	P6/P5	=	1.00000
49	37.596	981.45	125.019		A8	=	0.29682
5	38.343	979.95	125.019	57.308	A18	=	2.05950
8	38.343	979.95	125.019	57.308	XM8	=	0.61828
18	462.172	343.83	126.915	403.060	XM18	=	0.62235
					CD8	=	0.95408
Efficiencies:	isentr	polytr	RNI	P/P	CD18	=	0.94618
Outer LPC	0.6789	0.6885	0.871	1.240	PWX	=	50.00000
Inner LPC	0.6789	0.6824	0.871	1.000	V18/V8,id=	=	0.60806
IP Compressor	0.4215	0.4305	0.871	1.118	WBLD/W21	=	0.00000
HP Compressor	0.7768	0.8458	0.860	20.579	WBLD/W25	=	0.00000
Burner	1.0000			1.000	Loading %	=	34.33
HP Turbine	0.9047	0.8876	1.078	4.895	e444 th	=	0.87979
LP Turbine	0.8981	0.8821	0.383	3.848	WHcl/W25	=	0.06000
HP Spool mech	1.0000	Speed		48997.53	WLcl/W25	=	0.02000
LP Spool mech	1.0000	Speed		17142.90			
Bleed Air:	PBld = 2354.40	TBld = 901.1			ZWBld	=	0.00000
hum [%]	war0	FHV	Fuel				
0.0	0.00000	43.124	Generic				

B Engine Schematic

